A Kalman filter approach to virtual sensing for active noise control

Cornelis D. Petersen [a,*], Rufus Fraanje [b], Ben S. Cazzolato [a], Anthony C. Zander [a], Colin H. Hansen [a]

[a] *Active Noise and Vibration Control Group, School of Mechanical Engineering, The University of Adelaide, 5005 SA, Australia*

[b] *Delft Center for Systems and Control, Delft University of Technology, 2628 CD Delft, The Netherlands*

Abstract

Local active noise control systems aim to produce zones of quiet at a number of desired locations within a sound field, such as the ears of an observer. The resulting zones of quiet are usually centered at the error sensors, and are often too small to extend from the error sensors to the observer's ears. To overcome these problems, virtual sensing methods have been suggested. These methods are based on estimating the error signals at a number of locations remote from the physical locations of the error sensors. By minimising the estimated error signals, the zones of quiet can be moved away from the error sensors to the locations where noise control is desired, i.e. the virtual locations. In this paper, the active noise control problem under consideration is analysed using a state-space model of the plant. Kalman filtering theory is then used to develop a virtual sensing algorithm that computes optimal estimates of the error signals at the virtual locations. The developed algorithm is implemented on an acoustic duct arrangement, and the real-time estimation performance at a virtual location inside the acoustic duct is analysed. Furthermore,

the developed algorithm is combined with the filtered-x LMS, and the results of real-time broadband feedforward control experiments at the virtual location are presented.

Key words: virtual sensing, active noise control, Kalman filtering

PACS: 43.50.Ki

1 Introduction

Local active noise control systems aim to produce zones of quiet at a number of desired locations within a sound field, such as the ears of an observer. The resulting zones of quiet are usually centered at the error sensors, and are often too small to extend from the error sensors to the observer's ears [1]. To overcome these practical limitations, a number of virtual sensing methods for local active noise control systems have been suggested [2–12]. These methods can be used to obtain estimates of the error signals at locations remote from the physical locations of the error sensors. By choosing these remote locations to coincide with the desired locations of maximum attenuation, i.e. the *virtual locations*, estimates of the error signals at the observer's ears can be obtained without physically locating error sensors inconveniently close to the observer's head. This effectively creates *virtual sensors* at the virtual locations, and subsequent minimisation of the estimated *virtual error signals* by an active noise control algorithm results in zones of quiet that are moved away from the physical location of the error sensors to the desired locations of maximum attenuation.

* Corresponding author. Tel.:+61 8 8303 6940; fax: +61 8 8303 4367
Email address: cornelis.petersen@adelaide.edu.au (Cornelis D. Petersen).

The first virtual sensing algorithm that was suggested in the literature is called the *virtual microphone arrangement* [2]. In this algorithm, it is assumed that the primary disturbances at the virtual sensors, which are the disturbances that need to be attenuated, are equal to the primary disturbances at the physical sensors. This assumption can be made provided that the primary sound field changes relatively little between the physical and virtual sensors. This assumption is not made in a virtual sensing algorithm called the *remote microphone technique* [5,6], where an FIR or IIR filter matrix is used that computes an estimate of the primary disturbances at the virtual sensors from the primary disturbances at the physical sensors. In the virtual microphone arrangement [2], this filter matrix is assumed to be the identity matrix, and this algorithm is therefore a simplified version of the remote microphone technique. Both algorithms also require models of the secondary transfer paths between the control sources and the physical and virtual sensors. The required transfer path models are usually estimated in a preliminary identification stage by placing physical sensors at the virtual locations. In the virtual microphone arrangement [2] and the remote microphone technique [5,6], these transfer paths are modeled by FIR or IIR filter matrices.

The *adaptive LMS virtual microphone technique* [8,9] is another virtual sensing algorithm that has been proposed. In this algorithm, an array of physical sensors is used to obtain an estimate of the virtual error signal. This estimate is computed as a weighted summation of the physical error signals. The weights for each of the physical error signals are determined in a preliminary identification stage in which a physical sensor is placed at the virtual location. The difference between the error signal measured by this sensor and the estimated virtual error signal is then minimised by adjusting the weights using

the LMS algorithm [13]. After convergence of the weights, the physical sensor is removed from the virtual location, such that a virtual sensor is effectively created at this location.

Since the aim of the virtual sensing algorithm is to compute an accurate estimate of the virtual error signals, the problem of virtual sensing for active noise control can be formulated as a *linear estimation* problem [14]. In this paper, the virtual sensing problem is therefore analysed using a Kalman filtering approach. In this approach, the active noise control system under consideration is modeled by a state-space system whose outputs are the physical and virtual error signals. One of the major advantages of the state-space formulation over the transfer function formulation, which is employed in [2,5,6,12], is that there is no principle structural difference between the single- and the multi-channel case. The idea behind the Kalman filter approach taken here is that the information contained in the physical error signals can be used to compute estimates of the plant states, and the estimated plant states can be used to compute estimates of the virtual error signals. Furthermore, measurement noise on the physical sensors, including the ones that are placed at the virtual locations in a preliminary identification stage of the plant, can be conveniently included in the modeling of the problem, and its effect on the estimation performance of the virtual sensing algorithm can be analysed.

The main advantage of the proposed method over the virtual sensing methods introduced in [2,12] is that the assumption of equal primary disturbances at the physical and virtual sensors is not made. This therefore results in more accurate estimates of the virtual error signals, especially when the spatial change of the primary sound field between the physical and virtual sensors is significant and cannot be neglected. Another advantage over the methods

suggested in [2,5,6,8,12] is that the proposed algorithm is derived including measurement noise on the sensors, and that the effect of this measurement noise on the estimation performance is discussed. Also, the optimal estimation performance that can be obtained is analysed, showing that it is determined by the properties of the physical and virtual primary transfer paths. Furthermore, instead of using a number of FIR or IIR filter matrices to compute an estimate of the virtual error signals [2,5,6,12], the virtual sensing algorithm proposed here is described by one compact state-space model. The aim of this paper therefore is to present a more complete analysis of the virtual sensing problem, resulting in an algorithm that computes an estimate of the virtual error signals, in the presence of measurement noise, which is shown to be *optimal* in the least mean-square sense.

In Section 2, the active noise control problem under consideration is presented, and the notation and assumptions used in the analysis of the problem are introduced. In Section 3, it is assumed that physical sensors are temporarily located at the virtual locations in a preliminary identification stage of the active noise control system. A Kalman filter can then be formulated that computes optimal estimates of both the physical error signals measured by the physical sensors, and the virtual error signals measured by the physical sensors temporarily located at the virtual locations for system identification purposes. In Section 4, it is then assumed that the physical sensors located at the virtual locations in the preliminary identification stage have been removed. Using the presented Kalman filtering theory, a virtual sensing algorithm is then formulated that computes optimal estimates of the virtual error signals, assuming that only the physical error signals are directly measured. In Section 5, it is explained how the developed virtual sensing algorithm can be combined with the filtered-x

LMS algorithm [15], in order to minimise the estimated virtual error signals. In Section 6, the developed algorithm is implemented in real-time on an acoustic duct arrangement. The implemented algorithms are calculated in a preliminary identification stage, in which a state-space model of the plant is estimated using subspace model identification techniques [16,17]. The estimation performance and the broadband feedforward active noise control performance at a virtual location inside the duct are analysed.

2 Problem description

In this section, the notation and assumptions used in the analysis of the active noise control problem considered here are introduced. A block diagram of this problem is shown in Figure A.1.

[Fig. 1 about here.]

Note that the implementation illustrated in Figure A.1 was adopted in previous research into virtual sensing methods for active noise control [2–12]. The plant in this figure can be described by the following standard state-space model [14]

$$\begin{aligned} \mathbf{z}(n+1) &= \mathbf{A}\mathbf{z}(n) \ + \mathbf{B}_u\mathbf{u}(n) \ + \mathbf{B}_s\mathbf{s}(n) \\ \mathbf{e}_p(n) &= \mathbf{C}_p\mathbf{z}(n) + \mathbf{D}_{pu}\mathbf{u}(n) + \mathbf{D}_{ps}\mathbf{s}(n) + \mathbf{v}_p(n) \\ \mathbf{e}_v(n) &= \mathbf{C}_v\mathbf{z}(n) + \mathbf{D}_{vu}\mathbf{u}(n) + \mathbf{D}_{vs}\mathbf{s}(n) + \mathbf{v}_v(n), \end{aligned} \tag{1}$$

with $\mathbf{z}(n) \in \mathbb{R}^N$ the states of the plant, $\mathbf{s}(n) \in \mathbb{R}^S$ the disturbance source signals, $\mathbf{u}(n) \in \mathbb{R}^L$ the control signals, $\mathbf{e}_p(n) \in \mathbb{R}^{M_p}$ the physical error signals,

$\mathbf{e}_v(n) \in \mathbb{R}^{M_v}$ the virtual error signals that are not directly measured during real-time control, $\mathbf{v}_p(n) \in \mathbb{R}^{M_p}$ the physical measurement noise signals, and $\mathbf{v}_v(n) \in \mathbb{R}^{M_p}$ the virtual measurement noise signals. The virtual measurement noise signals are included to account for measurement noise on the physical sensors that are temporarily located at the virtual locations during a preliminary identification procedure of the considered active noise control system. The state-space matrices in Equation (1) are real-valued and of appropriate dimensions. Note that Equation (1) can be used to describe the input-output behaviour of any multiple input multiple output linear time-invariant active noise control system. The virtual sensing algorithm that will be derived here is therefore not restricted to the acoustic duct case that is considered in Section 6 to demonstrate the effectiveness of the proposed method in a practical situation, and can be implemented in more complicated three-dimensional sound fields, such as found inside more complex enclosures. The disturbance source signals $\mathbf{s}(n)$ are assumed to be *unknown* white and stationary random processes with zero-mean and unit covariance. The physical measurement noise signals $\mathbf{v}_p(n)$ and the virtual measurement noise signals $\mathbf{v}_v(n)$ are also assumed to be zero mean white and stationary random processes, such that the following covariance matrices can be defined [14]

$$\mathrm{E}\left[\begin{bmatrix}\mathbf{s}(n)\\ \mathbf{v}_p(n)\\ \mathbf{v}_v(n)\end{bmatrix}\begin{bmatrix}\mathbf{s}(k)\\ \mathbf{v}_p(k)\\ \mathbf{v}_v(k)\\ 1\end{bmatrix}^{\mathrm{T}}\right] = \left[\begin{array}{c|cc|c} \mathbf{I} & \mathbf{S}_{ps}^{\mathrm{T}} & \mathbf{S}_{vs}^{\mathrm{T}} & \mathbf{0} \\ \hline \mathbf{S}_{ps} & \mathbf{R}_p & \mathbf{R}_{pv} & \mathbf{0} \\ \mathbf{S}_{vs} & \mathbf{R}_{pv}^{\mathrm{T}} & \mathbf{R}_v & \mathbf{0} \end{array}\right] \delta_{nk}, \tag{2}$$

where E[·] denotes the expectation of the term inside brackets, $\mathbf{I} \in \mathbb{R}^{S \times S}$ is the identity matrix, and δ_{nk} the Kronecker delta function defined as

$$\delta_{nk} = \begin{cases} 1, \forall n = k \\ \\ 0, \, n \neq k. \end{cases} \tag{3}$$

In Equation (1), the term $\mathbf{B}_s\mathbf{s}(n)$ can be interpreted as process noise $\mathbf{w}(n)$, with $\mathbf{w}(n) \triangleq \mathbf{B}_s\mathbf{s}(n)$. The influence of the measurement noise signals and the direct feedthrough from the signals $\mathbf{s}(n)$ on the physical and virtual error signals can be combined into an auxiliary measurement noise signal $\mathbf{v}(n)$, which is defined as

$$\mathbf{v}(n) \triangleq \begin{bmatrix} \mathbf{D}_{ps}\mathbf{s}(n) + \mathbf{v}_p(n) \\ \\ \mathbf{D}_{vs}\mathbf{s}(n) + \mathbf{v}_v(n) \end{bmatrix}. \tag{4}$$

Using these definitions of the process noise signals $\mathbf{w}(n)$ and the auxiliary measurement noise signals $\mathbf{v}(n)$, the following covariance matrix can be defined

$$\mathrm{E}\left[\begin{bmatrix} \mathbf{w}(n) \\ \\ \mathbf{v}(n) \end{bmatrix}\begin{bmatrix} \mathbf{w}(k) \\ \\ \mathbf{v}(k) \end{bmatrix}^{\mathrm{T}}\right] = \left[\begin{array}{c|c} \bar{\mathbf{Q}}_s & \bar{\mathbf{S}}_s^{\mathrm{T}} \\ \hline \bar{\mathbf{S}}_s & \bar{\mathbf{R}} \end{array}\right] \delta_{nk}. \tag{5}$$

Using Equation (2), the covariance matrix $\bar{\mathbf{Q}}_s$ of the process noise $\mathbf{w}(n)$ is therefore given by

$$\bar{\mathbf{Q}}_s = \mathbf{B}_s\mathbf{B}_s^{\mathrm{T}}. \tag{6}$$

The covariance matrix $\bar{\mathbf{R}}$ of the auxiliary measurement noise $\mathbf{v}(n)$ on the physical and virtual sensors is defined as

$$\bar{\mathbf{R}} = \left[\begin{array}{c|c} \bar{\mathbf{R}}_p & \bar{\mathbf{R}}_{pv} \\ \hline \bar{\mathbf{R}}_{pv}^{\mathrm{T}} & \bar{\mathbf{R}}_v \end{array}\right], \tag{7}$$

and is given in expanded form by

$$\bar{\mathbf{R}} = \left[\begin{array}{c|c} \mathbf{R}_p + \mathbf{S}_{ps}\mathbf{D}_{ps}^{\mathrm{T}} + \mathbf{D}_{ps}\mathbf{S}_{ps}^{\mathrm{T}} + \mathbf{D}_{ps}\mathbf{D}_{ps}^{\mathrm{T}} & \mathbf{R}_{pv} + \mathbf{S}_{ps}\mathbf{D}_{vs}^{\mathrm{T}} + \mathbf{D}_{ps}\mathbf{S}_{vs}^{\mathrm{T}} + \mathbf{D}_{ps}\mathbf{D}_{vs}^{\mathrm{T}} \\ \hline \mathbf{R}_{pv}^{\mathrm{T}} + \mathbf{S}_{vs}\mathbf{D}_{ps}^{\mathrm{T}} + \mathbf{D}_{vs}\mathbf{S}_{ps}^{\mathrm{T}} + \mathbf{D}_{vs}\mathbf{D}_{ps}^{\mathrm{T}} & \mathbf{R}_v + \mathbf{S}_{vs}\mathbf{D}_{vs}^{\mathrm{T}} + \mathbf{D}_{vs}\mathbf{S}_{vs}^{\mathrm{T}} + \mathbf{D}_{vs}\mathbf{D}_{vs}^{\mathrm{T}} \end{array}\right]. \tag{8}$$

The covariance matrix $\bar{\mathbf{S}}_s$ between the auxiliary measurement noise $\mathbf{v}(n)$ and the process noise $\mathbf{w}(n)$ is given by

$$\bar{\mathbf{S}}_s = \begin{bmatrix} \bar{\mathbf{S}}_{ps} \\ \\ \bar{\mathbf{S}}_{vs} \end{bmatrix} = \begin{bmatrix} \mathbf{D}_{ps}\mathbf{B}_s^{\mathrm{T}} + \mathbf{S}_{ps}\mathbf{B}_s^{\mathrm{T}} \\ \\ \mathbf{D}_{vs}\mathbf{B}_s^{\mathrm{T}} + \mathbf{S}_{vs}\mathbf{B}_s^{\mathrm{T}} \end{bmatrix}. \tag{9}$$

The aim of the adaptive controller included in Figure A.1 is to compute a control signal $\mathbf{u}(n)$ that minimises the error signals $\mathbf{e}_v(n)$ at the virtual locations, where maximum noise reduction is desired. For this purpose, the adaptive controller generally requires the feedback information contained in the virtual error signals [15]. However, these signals are not directly measured during real-time control for the system considered here. The aim of the virtual sensing algorithm included in Figure A.1 is therefore to compute an accurate estimate $\hat{\mathbf{e}}_v(n)$ of the true virtual error signals, which can be calculated given the directly measured physical error signals $\mathbf{e}_p(n)$ and the deterministic control signals $\mathbf{u}(n)$. This estimate can then be used as a feedback signal to the adaptive controller to compute a control signal $\mathbf{u}(n)$ that minimises the estimated virtual error signals. If feedforward reference signals $\mathbf{x}(n)$ are available that are strongly correlated to the disturbance source signals $\mathbf{s}(n)$, an adaptive feedforward control algorithm can be used to minimise the estimated virtual error signals. If such signals are not available, an adaptive feedback control approach needs to be adopted.

3 Kalman filtering

In this section, it is assumed that physical sensors are temporarily located at the virtual locations in a preliminary identification stage of the plant defined in Equation (1), such that the virtual error signals are directly measured. A Kalman filter can then be formulated that computes optimal current estimates of the physical and virtual error signals.

The Kalman filter can be described in at least two forms, which are usually referred to as the *prediction* and *time-measurement update* forms [14]. The prediction form results in an estimate of the states $\mathbf{z}(n+1)$ given the observations $\mathbf{e}(i)$ of the physical and virtual error signals up to time $i = n$, with the state estimate denoted by $\hat{\mathbf{z}}(n+1|n)$, and with the error signals $\mathbf{e}(n) \in \mathbb{R}^{M_p+M_v}$ defined as

$$\mathbf{e}(n) = \begin{bmatrix} \mathbf{e}_p(n) \\ \\ \mathbf{e}_v(n) \end{bmatrix}. \tag{10}$$

Using the prediction form, the predicted state estimates $\hat{\mathbf{z}}(n+1|n)$ are computed as [14]

$$\hat{\mathbf{z}}(n+1|n) = (\mathbf{A} - \mathbf{K}_s\mathbf{C})\hat{\mathbf{z}}(n|n-1) + (\mathbf{B}_u - \mathbf{K}_s\mathbf{D}_u)\mathbf{u}(n) + \mathbf{K}_s\mathbf{e}(n), \tag{11}$$

with $\mathbf{K}_s \in \mathbb{R}^{N\times(M_p+M_v)}$ the Kalman gain matrix given by

$$\mathbf{K}_s = \begin{bmatrix} \tilde{\mathbf{K}}_{ps} & \tilde{\mathbf{K}}_{vs} \end{bmatrix}, \tag{12}$$

where tildes have been used on the Kalman gains to distinguish them from the Kalman gain matrix $\mathbf{K}_{ps}$ that will be introduced in Section 4. The matrices

$\mathbf{C}$ and $\mathbf{D}_u$ in Equation (11) are defined as

$$\mathbf{C} = \begin{bmatrix} \mathbf{C}_p \\ \\ \mathbf{C}_v \end{bmatrix}, \quad \mathbf{D}_u = \begin{bmatrix} \mathbf{D}_{pu} \\ \\ \mathbf{D}_{vu} \end{bmatrix}. \tag{13}$$

Predicted estimates $\hat{\mathbf{e}}(n|n-1) \in \mathbb{R}^{M_p+M_v}$ of the physical and virtual error signals are now computed, given the observations $\mathbf{e}(i)$ up to $i = n-1$, as

$$\hat{\mathbf{e}}(n|n-1) = \mathbf{C}\hat{\mathbf{z}}(n|n-1) + \mathbf{D}_u\mathbf{u}(n). \tag{14}$$

Using the above definitions, an *innovations* representation of the error signals $\mathbf{e}(n)$ is given by [14]

$$\begin{aligned} \hat{\mathbf{z}}(n+1|n) &= \mathbf{A}\hat{\mathbf{z}}(n|n-1) + \mathbf{B}_u\mathbf{u}(n) + \mathbf{K}_s\boldsymbol{\varepsilon}(n) \\ \mathbf{e}(n) &= \mathbf{C}\hat{\mathbf{z}}(n|n-1) + \mathbf{D}_u\mathbf{u}(n) + \boldsymbol{\varepsilon}(n), \end{aligned} \tag{15}$$

with $\boldsymbol{\varepsilon}(n) \in \mathbb{R}^{M_p+M_v}$ the *innovation* signals defined as

$$\boldsymbol{\varepsilon}(n) = \mathbf{e}(n) - \hat{\mathbf{e}}(n|n-1). \tag{16}$$

Note that the innovations representation defined in Equation (15) and the standard state-space model defined in Equation (1) result in error signals $\mathbf{e}(n)$ that have the same second order statistics [14].

The time-measurement update form of the Kalman filter results in a current estimate of the states $\mathbf{z}(n)$ given the observations $\mathbf{e}(i)$ of the physical and virtual error signals up to time $i = n$, with the current state estimate denoted by $\hat{\mathbf{z}}(n|n)$. The time-measurement update form is given by [14]

$$\hat{\mathbf{z}}(n|n) = (\mathbf{I} - \mathbf{M}_s\mathbf{C})\,\hat{\mathbf{z}}(n|n-1) - \mathbf{M}_s\mathbf{D}_u\mathbf{u}(n) + \mathbf{M}_s\mathbf{e}(n), \tag{17}$$

with $\mathbf{M}_s \in \mathbb{R}^{N\times(M_p+M_v)}$ the *innovation gain* matrix given by

$$\mathbf{M}_s = \begin{bmatrix} \tilde{\mathbf{M}}_{ps} \; \tilde{\mathbf{M}}_{vs} \end{bmatrix}. \tag{18}$$

The following theorem summarises the above discussions and defines an optimal solution for the Kalman gain matrix $\mathbf{K}_s$ that minimises

$$\mathrm{tr}\left(\mathrm{E}\left[\boldsymbol{\rho}(n|n-1)\boldsymbol{\rho}(n|n-1)^{\mathrm{T}}\right]\right), \tag{19}$$

with $\boldsymbol{\rho}(n|n-1) \in \mathbb{R}^N$ the *predicted* state estimation error defined as

$$\boldsymbol{\rho}(n|n-1) = \mathbf{z}(n) - \hat{\mathbf{z}}(n|n-1). \tag{20}$$

The theorem also defines an optimal solution for the innovation gain matrix $\mathbf{M}_s$ that minimises

$$\mathrm{tr}\left(\mathrm{E}\left[\boldsymbol{\rho}(n|n)\boldsymbol{\rho}(n|n)^{\mathrm{T}}\right]\right), \tag{21}$$

with $\boldsymbol{\rho}(n|n) \in \mathbb{R}^N$ the *current* state estimation error defined as

$$\boldsymbol{\rho}(n|n) = \mathbf{z}(n) - \hat{\mathbf{z}}(n|n). \tag{22}$$

A detailed proof of the presented theorem can be found in [14].

Theorem 1 (Kalman filter [14]) *Let a state-space realisation of the plant be given by Equation* (1)*, and let the covariance matrices* $\bar{\mathbf{Q}}_s$*,* $\bar{\mathbf{S}}_s$*, and* $\bar{\mathbf{R}}$ *be defined as in Equations* (6)–(9)*. Furthermore, let*

- *the pair* $(\mathbf{C}, \mathbf{A})$ *be detectable;*
- $\bar{\mathbf{R}} > 0$*,* $\bar{\mathbf{Q}}_s - \bar{\mathbf{S}}_s^{\mathrm{T}}\bar{\mathbf{R}}^{-1}\bar{\mathbf{S}}_s \geq 0$*;*
- $(\mathbf{A} - \bar{\mathbf{S}}_s^{\mathrm{T}}\bar{\mathbf{R}}^{-1}\mathbf{C}, \bar{\mathbf{Q}}_s - \bar{\mathbf{S}}_s^{\mathrm{T}}\bar{\mathbf{R}}^{-1}\bar{\mathbf{S}}_s)$ *has no uncontrollable modes on the unit circle.*

Then the time-measurement update form of the Kalman filter, which gives optimal current estimates $\hat{\mathbf{e}}(n|n)$ *of the physical and virtual error signals given*

observations $\mathbf{e}(i)$ *of the physical and virtual error signals up to* $i = n$*, is defined by the state-space realisation*

$$\left[\begin{array}{c} \hat{\mathbf{z}}(n+1|n) \\ \hline \hat{\mathbf{e}}(n|n) \end{array}\right] = \left[\begin{array}{c|cc} \mathbf{A} - \mathbf{K}_s\mathbf{C} & \mathbf{B}_u - \mathbf{K}_s\mathbf{D}_u & \mathbf{K}_s \\ \hline \mathbf{C} - \mathbf{C}\mathbf{M}_s\mathbf{C} & \mathbf{D}_u - \mathbf{C}\mathbf{M}_s\mathbf{D}_u & \mathbf{C}\mathbf{M}_s \end{array}\right] \left[\begin{array}{c} \hat{\mathbf{z}}(n|n-1) \\ \hline \mathbf{u}(n) \\ \\ \mathbf{e}(n) \end{array}\right], \quad (23)$$

where the Kalman gain matrix $\mathbf{K}_s$*, and the innovation gain matrix* $\mathbf{M}_s$ *are given by*

$$\begin{aligned} \mathbf{K}_s &= (\mathbf{A}\mathbf{P}_s\mathbf{C}^{\mathrm{T}} + \bar{\mathbf{S}}_s)\mathbf{R}_\varepsilon^{-1} \\ \mathbf{M}_s &= \mathbf{P}_s\mathbf{C}^{\mathrm{T}}\mathbf{R}_\varepsilon^{-1}, \end{aligned} \quad (24)$$

with $\mathbf{P}_s = \mathbf{P}_s^{\mathrm{T}} > 0$ *the unique stabilising solution to the discrete algebraic Ricatti equation (DARE) given by*

$$\mathbf{P}_s = \mathbf{A}\mathbf{P}_s\mathbf{A}^{\mathrm{T}} - (\mathbf{A}\mathbf{P}_s\mathbf{C}^{\mathrm{T}} + \bar{\mathbf{S}}_s^{\mathrm{T}})(\mathbf{C}\mathbf{P}_s\mathbf{C}^{\mathrm{T}} + \bar{\mathbf{R}})^{-1}(\mathbf{A}\mathbf{P}_s\mathbf{C}^{\mathrm{T}} + \bar{\mathbf{S}}_s^{\mathrm{T}})^{\mathrm{T}} + \bar{\mathbf{Q}}_s, \quad (25)$$

and where $\mathbf{R}_\varepsilon \in \mathbb{R}^{(M_p+M_v)\times(M_p+M_v)}$ *is the covariance matrix of the white innovation signals* $\boldsymbol{\varepsilon}(n)$ *defined in Equation* (16)*, which is given by*

$$\mathbf{R}_\varepsilon = \mathrm{E}[\boldsymbol{\varepsilon}(n)\boldsymbol{\varepsilon}(n)^{\mathrm{T}}] = \left[\begin{array}{cc} \tilde{\mathbf{R}}_{p\varepsilon} & \tilde{\mathbf{R}}_{pv\varepsilon} \\ \\ \tilde{\mathbf{R}}_{pv\varepsilon}^{\mathrm{T}} & \tilde{\mathbf{R}}_{v\varepsilon} \end{array}\right] = \mathbf{C}\mathbf{P}_s\mathbf{C}^{\mathrm{T}} + \bar{\mathbf{R}}. \quad (26)$$

4 Virtual output estimation

In this section, it is assumed that the physical sensors that are used to directly measure the virtual error signals in a preliminary identification stage of

the plant have been removed, or if present are only used to measure the performance of the virtual sensing algorithm. Using the Kalman filtering theory presented in Section 3, a virtual sensing algorithm can then be derived that computes optimal estimates of the virtual error signals.

4.1 Stochastic part of the plant

To simplify the discussions presented here, it is first assumed that the deterministic control signals are equal to zero, such that $\mathbf{u}(n) = 0$. For this case, the stochastic part of the plant can be written in innovations form, using Equation (15), as

$$\begin{aligned} \hat{\mathbf{z}}(n+1|n) &= \mathbf{A}\hat{\mathbf{z}}(n|n-1) + \tilde{\mathbf{K}}_{ps}\boldsymbol{\varepsilon}_p(n) + \tilde{\mathbf{K}}_{vs}\boldsymbol{\varepsilon}_v(n) \\ \mathbf{d}_p(n) &= \mathbf{C}_p\hat{\mathbf{z}}(n|n-1) + \boldsymbol{\varepsilon}_p(n) \\ \mathbf{d}_v(n) &= \mathbf{C}_v\hat{\mathbf{z}}(n|n-1) + \boldsymbol{\varepsilon}_v(n), \end{aligned} \tag{27}$$

where $\mathbf{d}_p(n)$ and $\mathbf{d}_v(n)$ are the primary physical and virtual disturbances, respectively. These primary disturbances are thus the error signals measured at the physical and virtual sensors when the controller is switched off. The input-output behavior of the state-space system in Equation (27) can be defined in transfer function form as

$$\begin{bmatrix} \mathbf{d}_p(n) \\ \\ \mathbf{d}_v(n) \end{bmatrix} = \begin{bmatrix} \tilde{\mathbf{G}}_{ps} \\ \\ \tilde{\mathbf{G}}_{vs} \end{bmatrix} \begin{bmatrix} \boldsymbol{\varepsilon}_p(n) \\ \\ \boldsymbol{\varepsilon}_v(n) \end{bmatrix}, \tag{28}$$

with state-space models of the transfer function matrices $\tilde{\mathbf{G}}_{ps} \in \mathcal{RH}_\infty^{M_p \times (M_p+M_v)}$ and $\tilde{\mathbf{G}}_{vs} \in \mathcal{RH}_\infty^{M_v \times (M_p+M_v)}$, with $\mathcal{RH}_\infty^{M \times N}$ the set of all asymptotically stable

rational $M \times N$ transfer function matrices [18], given by

$$\tilde{\mathbf{G}}_{ps} \sim \left[\begin{array}{c|cc} \mathbf{A} & \tilde{\mathbf{K}}_{ps} & \tilde{\mathbf{K}}_{vs} \\ \hline \mathbf{C}_p & \mathbf{I} & \mathbf{0} \end{array}\right], \quad \tilde{\mathbf{G}}_{vs} \sim \left[\begin{array}{c|cc} \mathbf{A} & \tilde{\mathbf{K}}_{ps} & \tilde{\mathbf{K}}_{vs} \\ \hline \mathbf{C}_v & \mathbf{0} & \mathbf{I} \end{array}\right]. \tag{29}$$

An estimate $\hat{\mathbf{d}}_v(n|n) \in \mathbb{R}^{M_v}$ of the virtual primary disturbances $\mathbf{d}_v(n)$ is now computed by filtering the physical primary disturbances $\mathbf{d}_p(n)$ with a filter $\mathbf{H} \in \mathcal{RH}_\infty^{M_v \times M_p}$, such that

$$\hat{\mathbf{d}}_v(n|n) = \mathbf{H}\mathbf{d}_p(n). \tag{30}$$

An optimal solution for the filter $\mathbf{H}$ is calculated by minimising the cost function

$$J = \operatorname{tr}\left(\mathrm{E}[\tilde{\boldsymbol{\varepsilon}}_v(n)\tilde{\boldsymbol{\varepsilon}}_v(n)^{\mathrm{T}}]\right), \tag{31}$$

with $\tilde{\boldsymbol{\varepsilon}}_v(n) \in \mathbb{R}^{M_v}$ the *virtual output errors* defined as

$$\tilde{\boldsymbol{\varepsilon}}_v(n) = \mathbf{d}_v(n) - \hat{\mathbf{d}}_v(n|n). \tag{32}$$

Using Equations (28)–(30) and Parseval's Theorem [15], an equivalent frequency domain expression of the cost function defined in Equation (31) is given by

$$J_\varepsilon = \|\mathbf{G}_{vs} - \mathbf{H}\mathbf{G}_{ps}\|_2^2, \tag{33}$$

with $\|\cdot\|_2$ the H_2-norm of the inside term [18], and where state-space realisations of the transfer function matrices $\mathbf{G}_{ps} = \tilde{\mathbf{G}}_{ps}\tilde{\mathbf{R}}_\varepsilon^{1/2}$ and $\mathbf{G}_{vs} = \tilde{\mathbf{G}}_{vs}\tilde{\mathbf{R}}_\varepsilon^{1/2}$

are defined as

$$\mathbf{G}_{ps} \sim \left[\begin{array}{c|cc} \mathbf{A} & \tilde{\mathbf{K}}_{ps}\tilde{\mathbf{R}}_{p\varepsilon}^{1/2} + \tilde{\mathbf{K}}_{vs}\tilde{\mathbf{R}}_{pv\varepsilon}^{1/2} & \tilde{\mathbf{K}}_{vs}\tilde{\mathbf{R}}_{v\varepsilon}^{1/2} \\ \hline \mathbf{C}_p & \tilde{\mathbf{R}}_{p\varepsilon}^{1/2} & \mathbf{0} \end{array}\right]$$
$$\mathbf{G}_{vs} \sim \left[\begin{array}{c|cc} \mathbf{A} & \tilde{\mathbf{K}}_{ps}\tilde{\mathbf{R}}_{p\varepsilon}^{1/2} + \tilde{\mathbf{K}}_{vs}\tilde{\mathbf{R}}_{pv\varepsilon}^{1/2} & \tilde{\mathbf{K}}_{vs}\tilde{\mathbf{R}}_{v\varepsilon}^{1/2} \\ \hline \mathbf{C}_v & \tilde{\mathbf{R}}_{pv\varepsilon}^{1/2} & \tilde{\mathbf{R}}_{v\varepsilon}^{1/2} \end{array}\right], \tag{34}$$

with $\tilde{\mathbf{R}}_{\varepsilon}^{1/2}$ a matrix such that

$$\tilde{\mathbf{R}}_{\varepsilon} = \tilde{\mathbf{R}}_{\varepsilon}^{1/2}\tilde{\mathbf{R}}_{\varepsilon}^{\mathrm{T}/2}, \tag{35}$$

where $\mathbf{R}_{\varepsilon}^{1/2}$ is defined as

$$\mathbf{R}_{\varepsilon}^{1/2} = \begin{bmatrix} \tilde{\mathbf{R}}_{p\varepsilon}^{1/2} & \mathbf{0} \\ \tilde{\mathbf{R}}_{pv\varepsilon}^{1/2} & \tilde{\mathbf{R}}_{v\varepsilon}^{1/2} \end{bmatrix}. \tag{36}$$

A block diagram of the considered optimisation problem is shown in Figure A.2.

[Fig. 2 about here.]

The following theorem defines a solution to this problem based on an outer-inner factorisation of $\mathbf{G}_{ps}$, in which $\mathbf{G}_{ps}$ is factorised into a stably invertible co-outer factor $\mathbf{G}_{ps,co}$ that is a minimum phase spectral factor of $\mathbf{G}_{ps}\mathbf{G}_{ps}^{*}$, and a co-inner factor $\mathbf{G}_{ps,ci}$ that only yields a phase shift. A detailed proof of the presented theorem can be found in [19].

Theorem 2 (Causal Wiener solution for H [19]) *Let state-space realisations of the transfer function matrices* $\mathbf{G}_{ps} \in \mathcal{RH}_{\infty}^{M_p \times (M_p + M_v)}$ *and* $\mathbf{G}_{vs} \in$

$\mathcal{RH}_\infty^{M_v\times(M_p+M_v)}$ *be given by Equation* (34)*, and assume that* $\mathbf{G}_{ps}$ *does not have any zeros on the unit circle. Then the following outer-inner factorisation can be defined [18]*

$$\mathbf{G}_{ps} = \mathbf{G}_{ps,co}\mathbf{G}_{ps,ci}, \tag{37}$$

where $\mathbf{G}_{ps,co}$ *has a stable left-inverse* $\mathbf{G}_{ps,co}^\dagger$*. Furthermore, let the complementary co-inner factor* $\mathbf{G}_{ps,ci}^\perp$ *be such that* $[\mathbf{G}_{ps,ci}^*\ \mathbf{G}_{ps,ci}^{\perp *}]^*$ *is unitary, with* $\mathbf{G}_{ps,ci}^*$ *the conjugate transpose of* $\mathbf{G}_{ps,ci}$*, and let* $[\cdot]_+$ *and* $[\cdot]_-$ *indicate the causal and anti-causal parts of the term inside the brackets. Then*

$$\mathbf{H}_o = \left[\mathbf{G}_{vs}\mathbf{G}_{ps,ci}^*\right]_+ \mathbf{G}_{ps,co}^\dagger \tag{38}$$

minimises

$$J = \|\mathbf{G}_{vs} - \mathbf{H}\mathbf{G}_{ps}\|_2^2, \quad \textit{subject to } \mathbf{H} \in \mathcal{RH}_\infty^{M_v\times M_p}, \tag{39}$$

and its minimum value is given by

$$J_{\min} = \|\mathbf{G}_{vs} - \mathbf{H}_o\mathbf{G}_{ps}\|_2^2 = \|\mathbf{G}_{vs}\mathbf{G}_{ps,ci}^{\perp *}\|_2^2 + \|[\mathbf{G}_{vs}\mathbf{G}_{ps,ci}^*]_-\|_2^2. \tag{40}$$

The minimum value of the cost function J defined in Equation (40) indicates that, theoretically, the estimation performance is determined by the properties of the primary transfer path matrices $\mathbf{G}_{ps}$ and $\mathbf{G}_{vs}$. The first term in Equation (40) contributes to the minimum value of the cost function when $\mathbf{G}_{vs}\mathbf{G}_{ps,ci}^{\perp *}$ is non-zero. This occurs when there are disturbances that contribute to the virtual primary disturbances $\mathbf{d}_v(n)$, but these disturbances are not observed at the physical sensors, and are thus not contained in the physical primary disturbances $\mathbf{d}_p(n)$ [19,20]. The virtual sensing algorithm is therefore not able to provide an estimate of this unobservable part of the virtual primary disturbances. The first term in Equation (40) is therefore related to the physical

and virtual sensor configuration that is used in the active noise control system. The locations of the physical sensors should thus be chosen such that all the modes that contribute to the virtual primary disturbances are observable at the physical sensors. The second term in Equation (40) is related to the restriction that the transfer function matrix $\mathbf{H}$ should be causal [19,20]. Therefore, the second term is determined by delays and non-minimum phase zeros in the physical primary transfer function matrix $\mathbf{G}_{ps}$, which contribute to the anti-causal terms in $\mathbf{G}^*_{ps,ci}$. To minimise the contribution of this second term, the physical and virtual sensor configuration should be chosen such that the physical primary disturbances contain *time-advanced* information about the virtual primary disturbances. This ensures that the virtual primary disturbances can be *causally* estimated from the physical primary disturbances.

In Appendix A, a minimal state-space realisation of the optimal filter solution $\mathbf{H}_o$ defined in Equation (38) is derived. Applying the theory presented in this appendix to the realisations of $\mathbf{G}_{ps}$ and $\mathbf{G}_{vs}$ defined in Equation (34), a minimal state-space realisation of $\mathbf{H}_o$ is given, similarly to Equation (A.18), by

$$\mathbf{H}_o \sim \left[\begin{array}{c|c} \mathbf{A}-\mathbf{K}\mathbf{C}_p & \mathbf{K} \\ \hline \mathbf{C}_v-\mathbf{M}\mathbf{C}_p & \mathbf{M} \end{array}\right], \tag{41}$$

where the matrices $\mathbf{K}$ and $\mathbf{M}$ are given by

$$\begin{aligned} \mathbf{K} &= (\mathbf{A}\mathbf{X}_s\mathbf{C}_p^{\mathrm{T}}+\mathbf{S})(\mathbf{C}_p\mathbf{X}_s\mathbf{C}_p^{\mathrm{T}}+\tilde{\mathbf{R}}_{p\varepsilon})^{-1}, \\ \mathbf{M} &= (\tilde{\mathbf{R}}_{pv\varepsilon}^{\mathrm{T}}+\mathbf{C}_v\mathbf{X}_s\mathbf{C}_p^{\mathrm{T}})(\mathbf{C}_p\mathbf{X}_s\mathbf{C}_p^{\mathrm{T}}+\tilde{\mathbf{R}}_{p\varepsilon})^{-1}, \end{aligned} \tag{42}$$

with $\mathbf{X}_s = \mathbf{X}_s^{\mathrm{T}} \geq 0$ is the stabilising solution to the DARE given by

$$\mathbf{X}_s = \mathbf{A}\mathbf{X}_s\mathbf{A}^{\mathrm{T}} - (\mathbf{A}\mathbf{X}_s\mathbf{C}_p^{\mathrm{T}}+\mathbf{S})(\mathbf{C}_p\mathbf{X}_s\mathbf{C}_p^{\mathrm{T}}+\mathbf{R})^{-1}(\mathbf{A}\mathbf{X}_s\mathbf{C}_p^{\mathrm{T}}+\mathbf{S})^{\mathrm{T}}+\mathbf{Q}, \tag{43}$$

where

$$\mathbf{Q} = \mathbf{K}_s \mathbf{R}_\varepsilon \mathbf{K}_s^{\mathrm{T}}, \quad \mathbf{S} = \mathbf{K}_s \begin{bmatrix} \tilde{\mathbf{R}}_{p\varepsilon} \\ \tilde{\mathbf{R}}_{pv\varepsilon}^{\mathrm{T}} \end{bmatrix}. \tag{44}$$

From Theorem 1, the matrices in Equations (42)–(44) can also be written as

$$\begin{aligned} \tilde{\mathbf{R}}_{pv\varepsilon}^{\mathrm{T}} &= \mathbf{C}_v \mathbf{P}_s \mathbf{C}_p^{\mathrm{T}} + \bar{\mathbf{R}}_{pv}^{\mathrm{T}}, \; \mathbf{Q} = \mathbf{A}\mathbf{P}_s\mathbf{A}^{\mathrm{T}} - \mathbf{P}_s + \bar{\mathbf{Q}}_s \\ \tilde{\mathbf{R}}_{p\varepsilon} &= \mathbf{C}_p \mathbf{P}_s \mathbf{C}_p^{\mathrm{T}} + \bar{\mathbf{R}}_p, \quad \mathbf{S} = \mathbf{A}\mathbf{P}_s\mathbf{C}_p^{\mathrm{T}} + \bar{\mathbf{S}}_{ps}^{\mathrm{T}}. \end{aligned} \tag{45}$$

Defining the matrix $\mathbf{P}_{ps} \triangleq \mathbf{P}_s + \mathbf{X}_s$, the matrices $\mathbf{K} \triangleq \mathbf{K}_{ps}$ and $\mathbf{M} \triangleq \mathbf{M}_{vs}$ in Equation (42) can thus also be written as

$$\begin{aligned} \mathbf{K}_{ps} &= (\mathbf{A}\mathbf{P}_{ps}\mathbf{C}_p^{\mathrm{T}} + \bar{\mathbf{S}}_{ps}^{\mathrm{T}})(\mathbf{C}_p\mathbf{P}_{ps}\mathbf{C}_p^{\mathrm{T}} + \bar{\mathbf{R}}_p)^{-1}, \\ \mathbf{M}_{vs} &= (\mathbf{C}_v\mathbf{P}_{ps}\mathbf{C}_p^{\mathrm{T}} + \bar{\mathbf{R}}_{pv}^{\mathrm{T}})(\mathbf{C}_p\mathbf{P}_{ps}\mathbf{C}_p^{\mathrm{T}} + \bar{\mathbf{R}}_p)^{-1}, \end{aligned} \tag{46}$$

where $\mathbf{P}_{ps} = \mathbf{P}_{ps}^{\mathrm{T}} > 0$ is the stabilising solution to the DARE given by

$$\mathbf{P}_{ps} = \mathbf{A}\mathbf{P}_{ps}\mathbf{A}^{\mathrm{T}} - (\mathbf{A}\mathbf{P}_{ps}\mathbf{C}_p^{\mathrm{T}} + \bar{\mathbf{S}}_{ps}^{\mathrm{T}})(\mathbf{C}_p\mathbf{P}_{ps}\mathbf{C}_p^{\mathrm{T}} + \bar{\mathbf{R}}_p)^{-1}(\mathbf{A}\mathbf{P}_{ps}\mathbf{C}_p^{\mathrm{T}} + \bar{\mathbf{S}}_{ps}^{\mathrm{T}})^{\mathrm{T}} + \bar{\mathbf{Q}}_s. \tag{47}$$

The DARE in the above equation is found by substituting the matrix relationships in Equation (45) into the DARE in Equation (43).

In summary, for the case that the deterministic control signals are equal to zero, a state-space realisation of the virtual sensing algorithm that computes an optimal current estimate $\hat{\mathbf{d}}_v(n|n)$ of the virtual primary disturbances given observations $\mathbf{d}_p(i)$ of the physical primary disturbances up to $i = n$ is defined

as

$$\left[\begin{array}{c} \hat{\mathbf{z}}(n+1|n) \\ \hline \hat{\mathbf{d}}_v(n|n) \end{array}\right] = \left[\begin{array}{c|c} \mathbf{A} - \mathbf{K}_{ps}\mathbf{C}_p & \mathbf{K}_{ps} \\ \hline \mathbf{C}_v - \mathbf{M}_{vs}\mathbf{C}_p & \mathbf{M}_{vs} \end{array}\right] \left[\begin{array}{c} \hat{\mathbf{z}}(n|n-1) \\ \hline \mathbf{d}_p(n) \end{array}\right], \tag{48}$$

where the Kalman gain matrix $\mathbf{K}_{ps}$ and the virtual gain matrix $\mathbf{M}_{vs}$ are given by Equation (46).

4.2 Including the deterministic part of the plant

In the previous section, the virtual sensing problem was analysed assuming that the deterministic control signals were equal to zero, and only the stochastic part of the plant was thus considered. In this section, it is assumed that the controller in Figure A.1 computes a control signal $\mathbf{u}(n)$, and it is explained how the deterministic part of the plant can be included into the virtual sensing algorithm presented in the previous section. The deterministic part of the state-space model of the plant in Equation (1) is given by

$$\begin{aligned} \mathbf{z}(n+1) &= \mathbf{A}\mathbf{z}(n) \;\; + \mathbf{B}_u\mathbf{u}(n) \\ \mathbf{y}_p(n) &= \mathbf{C}_p\mathbf{z}(n) + \mathbf{D}_{pu}\mathbf{u}(n) \\ \mathbf{y}_v(n) &= \mathbf{C}_v\mathbf{z}(n) + \mathbf{D}_{vu}\mathbf{u}(n), \end{aligned} \tag{49}$$

where $\mathbf{y}_p(n)$ and $\mathbf{y}_v(n)$ are the physical and virtual secondary disturbances, respectively. These secondary disturbances are thus the measurement noise free error signals at the physical and virtual sensors when the primary source is switched off. A current estimate $\hat{\mathbf{e}}_v(n|n)$ of the virtual error signals is now calculated by superposing the current estimate $\hat{\mathbf{d}}_v(n|n)$ of the virtual primary disturbances defined in Equation (30) and the virtual secondary disturbances

$\mathbf{y}_v(n)$, such that

$$\hat{\mathbf{e}}_v(n|n) = \hat{\mathbf{d}}_v(n|n) + \mathbf{y}_v(n) = \mathbf{H}_o\mathbf{d}_p(n) + \mathbf{y}_v(n), \tag{50}$$

with a state-space solution for the optimal filter $\mathbf{H}_o$ defined by Equation (48). Because the physical primary disturbances are given by $\mathbf{d}_p(n) = \mathbf{e}_p(n) - \mathbf{y}_p(n)$, Equation (50) can also be written as

$$\hat{\mathbf{e}}_v(n|n) = \begin{bmatrix} \mathbf{G}_{vu} - \mathbf{H}_o\mathbf{G}_{pu} & \mathbf{H}_o \end{bmatrix} \begin{bmatrix} \mathbf{u}(n) \\ \\ \mathbf{e}_p(n) \end{bmatrix}, \tag{51}$$

where state-space realisations of the transfer functions matrices $\mathbf{G}_{pu}$ and $\mathbf{G}_{vu}$ are defined from Equation (49) as

$$\mathbf{G}_{pu} \sim \left[\begin{array}{c|c} \mathbf{A} & \mathbf{B}_u \\ \hline \mathbf{C}_p & \mathbf{D}_{pu} \end{array}\right], \quad \mathbf{G}_{vu} \sim \left[\begin{array}{c|c} \mathbf{A} & \mathbf{B}_u \\ \hline \mathbf{C}_v & \mathbf{D}_{vu} \end{array}\right]. \tag{52}$$

Using the state-space realisations defined in Equations (48) and (52), it can be shown that a minimal state-space realisation of the transfer function matrix on the right-hand side of Equation (51) is given by

$$\begin{bmatrix} \mathbf{G}_{vu} - \mathbf{H}_o\mathbf{G}_{pu} & \mathbf{H}_o \end{bmatrix} \sim \left[\begin{array}{c|cc} \mathbf{A} - \mathbf{K}_{ps}\mathbf{C}_p & \mathbf{B}_u - \mathbf{K}_{ps}\mathbf{D}_{pu} & \mathbf{K}_{ps} \\ \hline \mathbf{C}_v - \mathbf{M}_{vs}\mathbf{C}_p & \mathbf{D}_{vu} - \mathbf{M}_{vs}\mathbf{D}_{pu} & \mathbf{M}_{vs} \end{array}\right]. \tag{53}$$

The presented discussion can now be summarised by the following theorem, in which the virtual sensing algorithm that includes both the deterministic and stochastic part of the plant is defined.

Theorem 3 (Virtual sensing algorithm) *Let a state-space realisation of the plant be given by Equation* (1)*, and let the covariance matrices* $\bar{\mathbf{Q}}_s$*,* $\bar{\mathbf{S}}_{ps}$*,*

$\bar{\mathbf{R}}_p$, *and* $\bar{\mathbf{R}}_{pv}$ *be defined as in Equations* (2)–(9). *Furthermore, let*

- *the pair* $(\mathbf{C}_p, \mathbf{A})$ *be detectable;*
- $\bar{\mathbf{R}}_p > 0$, $\bar{\mathbf{Q}}_s - \bar{\mathbf{S}}_{ps}^{\mathrm{T}} \bar{\mathbf{R}}_p^{-1} \bar{\mathbf{S}}_{ps} \geq 0$*;*
- $(\mathbf{A} - \bar{\mathbf{S}}_{ps}^{\mathrm{T}} \bar{\mathbf{R}}_p^{-1} \mathbf{C}_p, \bar{\mathbf{Q}}_s - \bar{\mathbf{S}}_{ps}^{\mathrm{T}} \bar{\mathbf{R}}_p^{-1} \bar{\mathbf{S}}_{ps})$ *has no uncontrollable modes on the unit circle.*

Then a state-space realisation of the virtual sensing algorithm that gives an optimal current estimate $\hat{\mathbf{e}}_v(n|n)$ *of the virtual error signals given observations* $\mathbf{e}_p(i)$ *of the physical error signals up to* $i = n$ *is defined as*

$$\left[\begin{array}{c} \hat{\mathbf{z}}(n+1|n) \\ \hline \hat{\mathbf{e}}_v(n|n) \end{array}\right] = \left[\begin{array}{c|cc} \mathbf{A} - \mathbf{K}_{ps}\mathbf{C}_p & \mathbf{B}_u - \mathbf{K}_{ps}\mathbf{D}_{pu} & \mathbf{K}_{ps} \\ \hline \mathbf{C}_v - \mathbf{M}_{vs}\mathbf{C}_p & \mathbf{D}_{vu} - \mathbf{M}_{vs}\mathbf{D}_{pu} & \mathbf{M}_{vs} \end{array}\right] \left[\begin{array}{c} \hat{\mathbf{z}}(n|n-1) \\ \hline \mathbf{u}(n) \\ \\ \mathbf{e}_p(n) \end{array}\right], \quad (54)$$

where the Kalman gain matrix $\mathbf{K}_{ps} \in \mathbb{R}^{N \times M_p}$ *and the virtual gain matrix* $\mathbf{M}_{vs} \in \mathbb{R}^{M_v \times M_p}$ *are given by*

$$\begin{aligned} \mathbf{K}_{ps} &= (\mathbf{A}\mathbf{P}_{ps}\mathbf{C}_p^{\mathrm{T}} + \bar{\mathbf{S}}_{ps}^{\mathrm{T}})\mathbf{R}_{p\varepsilon}^{-1}, \\ \mathbf{M}_{vs} &= (\mathbf{C}_v\mathbf{P}_{ps}\mathbf{C}_p^{\mathrm{T}} + \bar{\mathbf{R}}_{pv}^{\mathrm{T}})\mathbf{R}_{p\varepsilon}^{-1}, \end{aligned} \quad (55)$$

with $\mathbf{P}_{ps} = \mathbf{P}_{ps}^{\mathrm{T}} > 0$ *the unique stabilising solution to the DARE given by*

$$\mathbf{P}_{ps} = \mathbf{A}\mathbf{P}_{ps}\mathbf{A}^{\mathrm{T}} - (\mathbf{A}\mathbf{P}_{ps}\mathbf{C}_p^{\mathrm{T}} + \bar{\mathbf{S}}_{ps}^{\mathrm{T}})(\mathbf{C}_p\mathbf{P}_{ps}\mathbf{C}_p^{\mathrm{T}} + \bar{\mathbf{R}}_p)^{-1}(\mathbf{A}\mathbf{P}_{ps}\mathbf{C}_p^{\mathrm{T}} + \bar{\mathbf{S}}_{ps}^{\mathrm{T}})^{\mathrm{T}} + \bar{\mathbf{Q}}_s, \quad (56)$$

and where $\mathbf{R}_{p\varepsilon} \in \mathbb{R}^{M_p \times M_p}$ *is the covariance matrix of the white innovation signals* $\boldsymbol{\varepsilon}_p(n)$ *defined in Equation* (16), *which is given by*

$$\mathbf{R}_{p\varepsilon} = \mathrm{E}[\boldsymbol{\varepsilon}_p(n)\boldsymbol{\varepsilon}_p(n)^{\mathrm{T}}] = \mathbf{C}_p\mathbf{P}_{ps}\mathbf{C}_p^{\mathrm{T}} + \bar{\mathbf{R}}_p. \quad (57)$$

Comparing the state-space realisation of the virtual sensing algorithm defined in Theorem 3 with the state-space realisation of the Kalman filter defined in Theorem 1, it can be noted that the Kalman gain matrix $\mathbf{K}_{ps}$ defined in Equation (55) is equivalent to the Kalman gain matrix that would result if a Kalman filter was designed using Theorem 1 with only the physical error signals $\mathbf{e}_p(n)$ available for the computation of the state estimates. This is to be expected because the virtual error signals are not directly measured during real-time control and can therefore not be used to compute estimates of the plant states. Another interesting observation is that the virtual gain matrix $\mathbf{M}_{vs}$ defined in Equation (55) can also be written as

$$\mathbf{M}_{vs} = \mathbf{C}_v \mathbf{M}_{ps} + \bar{\mathbf{R}}_{pv}^{\mathrm{T}} \mathbf{R}_{p\varepsilon}^{-1}, \tag{58}$$

with the innovation gain matrix $\mathbf{M}_{ps}$ given by

$$\mathbf{M}_{ps} = \mathbf{P}_{ps} \mathbf{C}_p^{\mathrm{T}} \mathbf{R}_{p\varepsilon}^{-1}. \tag{59}$$

Again, it can be seen that the innovation gain matrix $\mathbf{M}_{ps}$ defined in Equation (59) is equivalent to the innovation gain matrix that would result if a Kalman filter was designed in time-measurement update form using Theorem 1 with only the physical error signals $\mathbf{e}_p(n)$ available for computing the current state estimates. In other words, if the auxiliary measurement noise signals on the physical and virtual sensors are uncorrelated, such that $\bar{\mathbf{R}}_{pv} = \mathbf{0}$ in Equation (7), the virtual gain matrix defined in Equation (58) is equal to $\mathbf{M}_{vs} = \mathbf{C}_v \mathbf{M}_{ps}$. For this case, the current estimate of the virtual error signals

is calculated from Equation (54) as

$$\hat{\mathbf{e}}_v(n|n) = (\mathbf{C}_v - \mathbf{M}_{vs}\mathbf{C}_p)\hat{\mathbf{z}}(n|n-1) + (\mathbf{D}_{vu} - \mathbf{C}_v\mathbf{M}_{ps}\mathbf{D}_{pu})\mathbf{u}(n) + \mathbf{C}_v\mathbf{M}_{ps}. \quad (60)$$

Comparing this equation to Equation (17), it can thus be seen that

$$\hat{\mathbf{e}}_v(n|n) = \mathbf{C}_v\hat{\mathbf{z}}(n|n) + \mathbf{D}_{vu}\mathbf{u}(n), \quad (61)$$

with $\hat{\mathbf{z}}(n|n)$ the current estimate of the states calculated given observations $\mathbf{e}_p(i)$ of the physical error signals up to time $i = n$. This result is intuitive, because when the auxiliary measurement noise signals on the physical and virtual sensors are uncorrelated, the auxiliary measurement noise signals on the virtual sensors cannot be predicted from the physical error signals. In other words, for this case the physical error signals only contain information that can be used to compute current state estimates $\hat{\mathbf{z}}(n|n)$, and a current estimate $\hat{\mathbf{e}}_v(n|n)$ of the virtual error signals is then computed as defined in Equation (61).

5 Filtered-x LMS algorithm

As illustrated in Figure A.1, the final aim of the active noise control system considered here is to minimise the current estimate of the virtual error signals, such that the zones of quiet are moved away from the physical sensors to the virtual locations where maximum noise reduction is desired. In the acoustic duct experiments presented in Section 6, it is assumed that a feedforward reference signal $x(n)$ is available, and the filtered-x LMS algorithm [15] is used to minimise the current estimate of the virtual error signal. It is now explained how this algorithm can be combined with the virtual sensing algorithm pre-

sented in Section 4. To keep the discussion simple, it is assumed that there is only one control source, one feedforward reference signal, and one virtual error signal. A detailed discussion of the filtered-x LMS algorithm for the multiple reference MIMO case can be found in [15].

For the active noise control problem considered here, the filtered-x LMS algorithm is given by [15]

$$\begin{aligned} u(n) &= \mathbf{w}(n)^{\mathrm{T}}\mathbf{x}(n), \\ \mathbf{w}(n+1) &= \mathbf{w}(n) - \mu\mathbf{r}_v(n)\hat{e}_v(n|n), \end{aligned} \tag{62}$$

with $\mu \in \mathbb{R}^+$ the convergence coefficient, $\hat{e}_v(n|n)$ the current estimate of the virtual error signal, $\mathbf{w}(n) \in \mathbb{R}^I$ a vector of filter coefficients given by

$$\mathbf{w}(n) = \begin{bmatrix} w_0(n) \; w_1(n) \; \ldots \; w_{I-1}(n) \end{bmatrix}^{\mathrm{T}}, \tag{63}$$

$\mathbf{x}(n) \in \mathbb{R}^I$ a vector of feedforward reference signals defined as

$$\mathbf{x}(n) = \begin{bmatrix} x(n) \; x(n-1) \; \ldots \; x(n-I+1) \end{bmatrix}^{\mathrm{T}}, \tag{64}$$

and $\mathbf{r}_v(n) \in \mathbb{R}^I$ a vector given by

$$\mathbf{r}_v(n) = \begin{bmatrix} r_v(n) \; r_v(n-1) \; \ldots \; r_v(n-I+1) \end{bmatrix}^{\mathrm{T}}, \tag{65}$$

with $r_v(n)$ the virtual filtered-reference signal. This signal is generated by filtering the feedforward reference signal $x(n)$ with the virtual secondary transfer path G_{vu}, such that

$$r_v(n) = G_{vu}x(n), \tag{66}$$

with a state-space realisation of the secondary virtual transfer path G_{vu} defined in Equation (52). In the real-time experiments presented in the next

section, a state-space model of this transfer path is used to generate the virtual filtered-reference signal.

6 Acoustic duct experiments

The algorithms introduced in the previous sections were implemented on an acoustic duct arrangement. This arrangement is now described after which experimental results are presented and discussed.

6.1 Experimental arrangement

Figure A.3 shows a schematic diagram of the rigidly terminated rectangular acoustic duct that was used in the real-time experiments. The acoustic duct has length $L = 4.830\,\mathrm{m}$, width $0.205\,\mathrm{m}$, and height $0.205\,\mathrm{m}$.

[Fig. 3 about here.]

A $4''$ loudspeaker located at $x_p = 4.730\,\mathrm{m}$ is used as a primary disturbance source and another $4''$ loudspeaker located at $x_s = 0.100\,\mathrm{m}$ as a control source. The input signal to the primary loudspeaker is a white noise signal filtered by an 8^{th} order Butterworth filter with a pass-band between 50–500 Hz. This signal is also used as a feedforward reference signal $x(n)$ in the filtered-x LMS algorithm. An electret microphone located at $x_{ph} = 1.475\,\mathrm{m}$ is used as a physical sensor. The virtual location is chosen as $x_v = 1.575\,\mathrm{m}$ at a distance of $10.0\,\mathrm{cm}$ from the physical sensor. This distance proved to be large enough to demonstrate the effectiveness of the proposed method. An electret microphone is positioned at the considered virtual location, which is used in a preliminary

identification stage of the plant described in Section 6.2 and also to measure the performance of the implemented virtual sensing and active noise control algorithms. To implement the developed algorithms in real-time, the host-target software program xPC Target® is used. A sampling frequency of $f_s = 1.6\,\text{kHz}$ is employed in the real-time experiments.

6.2 Preliminary identification stage

Subspace model identification techniques [16,17] are used to estimate a state-space model of the acoustic duct arrangement in innovations form, which is defined from Equation (15) as

$$\begin{aligned} \hat{\mathbf{z}}(n+1|n) &= \mathbf{A}\hat{\mathbf{z}}(n|n-1) + \mathbf{B}_u u(n) + \mathbf{K}_s \boldsymbol{\varepsilon}(n) \\ \mathbf{e}(n) &= \mathbf{C}\hat{\mathbf{z}}(n|n-1) + \mathbf{D}_u u(n) + \boldsymbol{\varepsilon}(n). \end{aligned} \tag{67}$$

Given measured input-output data $\{u(n), \mathbf{e}(n)\}_{n=1}^{N_s}$, the objective of subspace model identification is to estimate the state-space matrices $(\mathbf{A}, \mathbf{B}_u, \mathbf{C}, \mathbf{D}_u)$ and the Kalman gain matrix $\mathbf{K}_s$) up to a similarity transformation, and the covariance matrix $\mathbf{R}_\varepsilon = \mathrm{E}[\boldsymbol{\varepsilon}(n)\boldsymbol{\varepsilon}(n)^{\mathrm{T}}]$ of the innovation signals. A minimum-phase relationship between the innovation signals $\boldsymbol{\varepsilon}(n)$ and the error signals $\mathbf{e}(n)$ is guaranteed by constraining the eigenvalues of $\mathbf{A} - \mathbf{K}_s\mathbf{C}$ to be inside the unit circle. Several subspace identification algorithms have been proposed [16,17,21], which are all based on numerically reliable algorithms such as the QR-factorisation and singular value decomposition. In the acoustic duct experiments presented here, a subspace model identification algorithm called SSARX proposed in [22] is used.

A two-step identification procedure is used in the experiments, in which the deterministic part and the stochastic part of the plant are identified separately by setting the input signal into the primary loudspeaker equal to zero in the first step, such that $s(n) = 0$, and the control signal equal to zero in the second step, such that $u(n) = 0$. A one step approach in which a full model of the plant is estimated at once could also be used, but a two-step approach usually results in a more accurate model of the true plant [19]. The two-step identification procedure and results are now described.

In the first step, a state-space model of the deterministic part of the plant, which was defined in Equation (49), is identified by switching off the input signal into the primary loudspeaker. An input/output data-set

$$\{u(n), \begin{bmatrix} y_p(n) \\ \\ y_v(n) \end{bmatrix}\}_{n=1}^{32000} \tag{68}$$

is recorded, with $y_p(n)$ the measured physical secondary disturbance, $y_v(n)$ the measured virtual secondary disturbance, and $u(n)$ the input signal into the control source given by the band-pass filtered white noise signal described in the previous section. The recorded data-set is divided into a training data-set and a validation data-set each 16000 samples long. The accuracy of the estimated model is expressed by the variance-accounted-for (VAF) value, which is defined as [19]

$$\text{VAF} = \frac{1}{2}\sum_{m=1}^{2}\left[\max\left(1 - \frac{\text{var}(\mathbf{Y}_m - \hat{\mathbf{Y}}_m)}{\text{var}(\mathbf{Y}_m)}, 0\right) \times 100\%\right], \tag{69}$$

where $\text{var}(\cdot)$ is the variance of the data sequence between parentheses, $\mathbf{Y} \in \mathbb{R}^{16000\times 2}$ is the output validation data-set, and $\hat{\mathbf{Y}} \in \mathbb{R}^{16000\times 2}$ is the data-set resulting from filtering the input validation data-set with the estimated state-

space model. The VAF value in Equation (69) is 100% if the matrices $\mathbf{Y}$ and $\hat{\mathbf{Y}}$ are identical, and decreases as the difference in these matrices becomes greater. In the final experiments, a state-space model of the deterministic part of the plant of order 32 is estimated, which gives a VAF = 99.9% on the validation data-set.

[Fig. 4 about here.]

In Figure A.4, the Bode diagram of the estimated state-space model is compared with the frequency response functions between the control input signal and the measured physical and virtual secondary disturbances, which are calculated from the validation data-set. This figure shows that a good fit on the validation data is obtained in the frequency band of interest between 50–500 Hz. The high magnitudes at frequencies outside this band occur because the computer generated input signal has very little energy at these frequencies while there still is some measurement noise at these frequencies.

In the second step, the control signal is set to zero, and an innovations model of the stochastic part of the plant, which was defined in Equation (27), is identified using a stochastic subspace identification algorithm [22]. An output data-set

$$\left\{ \begin{bmatrix} d_p(n) \\ \\ d_v(n) \end{bmatrix} \right\}_{n=1}^{32000} \tag{70}$$

is recorded, with $d_p(n)$ and $d_v(n)$ the measured primary physical and virtual disturbances, respectively. The recorded data-set is divided into a training data-set and a validation data-set each 16000 samples long. The accuracy of the estimated innovations model is evaluated by calculating the VAF value

based on the validation output data-set and the predicted estimates $\hat{\mathbf{d}}(n|n-1)$ of the output. From Equations (11) and (14), with the control signal $\mathbf{u}(n) = 0$, these predicted estimates are calculated as

$$\begin{aligned} \hat{\mathbf{z}}(n+1|n) &= (\hat{\mathbf{A}} - \hat{\mathbf{K}}_s\hat{\mathbf{C}})\hat{\mathbf{z}}(n|n-1) + \hat{\mathbf{K}}_s\mathbf{d}(n) \\ \hat{\mathbf{d}}(n|n-1) &= \hat{\mathbf{C}}\hat{\mathbf{z}}(n|n-1), \end{aligned} \tag{71}$$

with $\hat{\mathbf{A}}$, $\hat{\mathbf{C}}$, and $\hat{\mathbf{K}}_s$ the state-space matrices that are computed using stochastic subspace identification, and where $\mathbf{d}(n) = [d_p(n)\ d_v(n)]^{\mathrm{T}}$. In the final experiments, a 40^{th} order stochastic innovations model is estimated on the training data-set. For the physical primary disturbances, a VAF = 99.7% is obtained on the validation data-set, while for the virtual primary disturbances, a VAF = 98.8% is obtained on the validation data-set.

Using the identified model of the stochastic part of the plant, the state-space realisation in Equation (48) is calculated as described in Section 4.1. This state-space realisation computes an optimal current estimate $\hat{d}_v(n|n)$ of the virtual primary disturbance given observations $d_p(i)$ of the physical primary disturbance up to $i = n$. This state-space model and the state-space model of the deterministic part of the plant estimated in the first step of the identification procedure are then used to compute the virtual sensing algorithm described in Section 4. This algorithm is implemented on the acoustic duct arrangement.

The broadband estimation performance of the implemented virtual sensing algorithm is analysed with the controller switched off. For this case, the virtual output error was defined in Equation (32) as $\tilde{\varepsilon}_v(n) = d_v(n) - \hat{d}_v(n|n)$.

[Fig. 5 about here.]

In Figure A.5, the power spectra of the measured virtual primary disturbance $d_v(n)$ and the virtual output error $\tilde{\varepsilon}_v(n)$ are plotted. These power spectra are generated by averaging over 50 computed power spectra. The overall mean square value of the measured virtual primary disturbance is 100.0 dB re 20 μPa, and the overall mean square value of the virtual output error is 75.4 dB re 20 μPa, which is a difference of 24.6 dB. The power spectrum of the virtual output error in Figure A.5 shows that an accurate estimate of the virtual primary disturbance $d_v(n)$ is obtained over the entire frequency band of interest between 50-500 Hz.

The filtered-x LMS algorithm described in Section 5 is implemented on the acoustic duct arrangement to analyse the broadband adaptive feedforward control performance that can be obtained at the virtual location. The filtered-x LMS algorithm is implemented using a convergence coefficient $\mu = 5 \cdot 10^{-6}$ and $I = 450$ filter coefficients. The control performance obtained at the virtual location while minimising the current estimate $\hat{e}_v(n|n)$ of the virtual error signal is compared with the control performance obtained at the virtual location while minimising the true virtual error signal $e_v(n)$ directly measured during real-time control by the electret microphone located at the considered virtual location. For both cases, the control performance is measured after conver-

gence of the adaptive algorithm. The results are shown in Figure A.6, where the power spectrum of the measured virtual primary disturbance $d_v(n)$, and the power spectra of the residual error signal at the virtual location measured after convergence of the adaptive controller for both control cases are plotted.

[Fig. 6 about here.]

These power spectra are generated by averaging over 50 computed power spectra. An overall attenuation of 19.7 dB is obtained while minimising the current estimate of the virtual error signal, compared to an overall attenuation of 25.1 dB obtained while minimising the true virtual error signal directly measured at the virtual location, which is a difference of 5.4 dB. One reason for this difference, which follows from the discussion presented after Theorem 2, is that a perfect current estimate of the virtual primary disturbance can only be computed from the physical primary disturbance if these disturbances are completely causally related, which is not the case for the physical and virtual sensor configuration considered here. Another reason is that when the virtual error signal is directly measured during real-time control, the filtered-x LMS algorithm can partly compensate for small, and generally unavoidable, errors in the estimate of the virtual secondary transfer path G_{vu} that is used in Equation (66) to generate the virtual filtered-reference signal, whereas this is not the case if the virtual error signal is estimated using a virtual sensing algorithm [6]. The attenuation is therefore expected to be slightly different at the deep anti-resonance frequencies in the virtual secondary transfer path (see Figure A.4), since the accuracy of the estimated model is generally poorest at these frequencies [23].

[Fig. 7 about here.]

The performance obtained at the virtual location while minimising the current estimate $\hat{e}_v(n|n)$ of the virtual error signal is also compared with the performance obtained at this location while minimising the physical error signal $e_p(n)$. The minimisation of the physical error signal is achieved using the filtered-x LMS algorithm, which is again implemented using a convergence coefficient $\mu = 5 \cdot 10^{-6}$ and $I = 450$ filter coefficients. The control performance obtained at the physical sensor is shown in Figure A.7(a), where the power spectra of the physical primary disturbance and the residual physical error signal measured after convergence of the adaptive controller are plotted. These power spectra are generated by averaging over 50 computed power spectra. An overall attenuation of 25.0 dB is obtained at the physical sensor. Figure A.7(b) shows the power spectra of the virtual primary disturbance, the residual virtual error signal obtained while minimising the current estimate $\hat{e}_v(n|n)$ of the virtual error signal, and the residual virtual error signal obtained while minimising the physical error signal $e_p(n)$. Although an overall attenuation of 25.0 dB was obtained at the physical sensor, the virtual primary disturbance at the virtual location was actually amplified by 1.4 dB. Thus, minimising the current estimate of the virtual error signal instead of the physical error signal increased the overall attenuation obtained at the virtual location by 21 dB. This result illustrates the potential benefits of adopting the proposed virtual sensing method over a conventional sensing method, and indicates that the distance between the physical and virtual sensors is large enough to demonstrate the effectiveness of the proposed method.

7 Conclusion

A virtual sensing algorithm for local active noise control systems has been derived using Kalman filtering theory. The developed algorithm computes an optimal current estimate of the error signals at locations remote from the error sensors and can be used when the desired locations of noise reduction need to be moved away from the physical locations of the error sensors. To demonstrate the effectiveness of the proposed method in a practical situation, the developed algorithm has been implemented on an acoustic duct arrangement. The real-time broadband estimation and adaptive feedforward control performance obtained at a virtual location inside the acoustic duct have been analysed. The experimental results showed that an accurate estimate of the virtual error signal was obtained over a broad frequency range, and that subsequent minimisation of the estimated virtual error signal resulted in an overall broadband attenuation of the unwanted noise at the virtual location of 19.7 dB. Because the proposed virtual sensing algorithm has been derived given a state-space model that describes the input-output behaviour of a general multiple input multiple output active noise control system, the proposed method can also be applied to other cases such as three-dimensional sound fields inside more complex enclosures.

Acknowledgements

The authors gratefully acknowledge the University of Adelaide for providing an ASI scholarship, and the Australian Research Council for supporting this research. The work of R. Fraanje has been supported by the 'Intelligent Ma-

terials for Active Noise Reduction' (InMAR) project, funded under the 6th Framework Programme of the European Commission.

References

[1] S. J. Elliott, P. Joseph, A. J. Bullmore, P. A. Nelson, Active cancellation at a point in a pure tone diffuse sound field, Journal of Sound and Vibration 120 (1) (1988) 183–189.

[2] S. J. Elliott, A. David, A virtual microphone arrangement for local active sound control, Proceedings of the 1st International Conference on Motion and Vibration Control, Yokohama, Japan, 1992, pp. 1027–1031.

[3] J. Garcia-Bonito, S. J. Elliott, C. C. Boucher, A virtual microphone arrangement in a practical active headrest, Proceedings of Inter-Noise '96, Liverpool, UK, 1996, pp. 1115–1120.

[4] J. Garcia-Bonito, S. J. Elliott, C. C. Boucher, Generation of zones of quiet using a virtual microphone arrangement, Journal of the Acoustical Society of America 101 (6) (1997) 3498–3516.

[5] S. R. Popovich, Active acoustic control in remote regions, US Patent No. 5,701,350 (December 23 1997).

[6] A. Roure, A. Albarrazin, The remote microphone technique for active noise control, Proceedings of Active '99, Ft Lauderdale, Florida, USA, 1999, pp. 1233–1244.

[7] J. Yuan, Virtual sensing for broadband noise control in a lightly damped enclosure, Journal of the Acoustical Society of America 116 (2) (2004) 934–941.

[8] B. S. Cazzolato, An adaptive LMS virtual microphone, Proceedings of Active '02, ISVR, Southampton, UK, 2002, pp. 105–116.

[9] J. M. Munn, Virtual sensors for active noise control, Ph.D. thesis, Department of Mechanical Engineering, The University of Adelaide, SA 5005 (July 17 2003).

[10] M. Pawelczyk, Multiple input- multiple output adaptive feedback control strategies for the active headrest system: design and real-time implementation, International Journal of Adaptive Control and Signal Processing 17 (10) (2003) 785–800.

[11] M. Pawelczyk, Design and analysis of a virtual-microphone active noise control system, Proceedings of the 12$^{\text{th}}$ International Congress on Sound and Vibration, Lisbon, Portugal, 2005, pp. 1–8.

[12] S. M. Kuo, W. S. Gan, Active noise control systems with optimized secondary path, Proceedings of the International Conference on Control Applications, Taipei, Taiwan, 2004, pp. 765–770.

[13] S. Haykin, Adaptive Filter Theory, 4$^{\text{th}}$ Edition, Prentice Hall, Upper Saddle River, New Jersey, USA, 2002.

[14] T. Kailath, A. H. Sayed, B. Hassibi, Linear estimation, Prentice Hall, Upper Saddle River, N. J., 2000.

[15] S. J. Elliott, Signal Processing for Active Control, 1st Edition, Academic Press, 2001.

[16] P. van Overschee, B. de Moor, Subspace Identification for Linear Systems: Theory, Implementation, Applications, Kluwer Academic Publishers, Boston, MA, USA, 1996.

[17] L. R. J. Haverkamp, State space identification: Theory and practice, Ph.D. thesis, System and Control Engineering Group, Delft University of Technology, The Netherlands (2001).

[18] K. Zhou, J. C. Doyle, K. Glover, Robust and Optimal Control, Prentice-Hall, Inc., Upper Saddle River, New Jersey, USA, 1996.

[19] P. R. Fraanje, Robust and fast schemes in active noise and vibration control, Ph.D. thesis, University of Twente, The Netherlands (2004).

[20] C. D. Petersen, A. C. Zander, B. S. Cazzolato, R. Fraanje, C. H. Hansen, Limits on active noise control performance at virtual error sensors, Proceedings of Active '06, Adelaide, South Australia, Australia, 2006, pp. 1233–1244.

[21] J. Mari, P. Stoica, T. McKelvey, Vector ARMA estimation: A reliable subspace approach, IEEE Transactions on Signal Processing 48 (7) (2000) 2092–2104.

[22] M. Jansson, Subspace identification and ARX modeling, Proceedings of the 13th IFAC Symposium on System Identification (SYSID), Rotterdam, The Netherlands, 2003, pp. 1625–1630.

[23] V. Verdult, R. Fraanje, SLICOT determines models for active noise control, NICONET Newsletter, no. 8, Working Group on Software, http://www.win.tue.nl/niconet, 2002, pp. 13–18.

[24] V. Ionescu, C. Oară, M. Weiss, Generalized Riccati Theory and Robust Control: A Popov Function Approach, John Wiley & Sons, Chichester, England, 1999.

A Derivation of a minimal realisation of $\mathbf{H}_o$

Let minimal state-space realisations of the transfer function matrices $\mathbf{G}_{ps}$ and $\mathbf{G}_{vs}$ be given by

$$\mathbf{G}_{ps} \sim \left[\begin{array}{c|c} \mathbf{A} & \mathbf{B}_s \\ \hline \mathbf{C}_p & \mathbf{D}_{ps} \end{array}\right], \quad \mathbf{G}_{vs} \sim \left[\begin{array}{c|c} \mathbf{A} & \mathbf{B}_s \\ \hline \mathbf{C}_v & \mathbf{D}_{vs} \end{array}\right]. \tag{A.1}$$

Then a minimal realisation of the transfer function matrix $\mathbf{H}_o$ in Equation (38) can be derived as follows.

Outer-inner factorisation of $\mathbf{G}_{ps}$

Assuming that $\mathbf{G}_{ps}$ has no zeros on the unit circle, state-space realisations of the co-outer factor $\mathbf{G}_{ps,co}$, and the co-inner factor $\mathbf{G}_{ps,ci}$ are given by [24]

$$\mathbf{G}_{ps,co} \sim \left[\begin{array}{c|c} \mathbf{A} & \mathbf{K}\mathbf{D}_{ps}^{co} \\ \hline \mathbf{C}_p & \mathbf{D}_{ps}^{co} \end{array}\right], \quad \mathbf{G}_{ps,ci} \sim \left[\begin{array}{c|c} \mathbf{A}-\mathbf{K}\mathbf{C}_p & \mathbf{B}-\mathbf{K}\mathbf{D}_{ps} \\ \hline \mathbf{D}_{ps}^{co\dagger}\mathbf{C}_p & \mathbf{D}_{ps}^{co\dagger}\mathbf{D}_{ps} \end{array}\right], \tag{A.2}$$

where $\mathbf{D}_{ps}^{co}$ is calculated such that

$$\mathbf{D}_{ps}^{co}\mathbf{D}_{ps}^{co\mathrm{T}} = \mathbf{C}_p\mathbf{X}_s\mathbf{C}_p^{\mathrm{T}} + \mathbf{R}, \tag{A.3}$$

and where the matrix $\mathbf{K}$ is defined as

$$\mathbf{K} = (\mathbf{A}\mathbf{X}_s\mathbf{C}_p^{\mathrm{T}} + \mathbf{S})(\mathbf{C}_p\mathbf{X}_s\mathbf{C}_p^{\mathrm{T}} + \mathbf{R})^{-1}, \tag{A.4}$$

with the matrix $\mathbf{X}_s = \mathbf{X}_s^{\mathrm{T}} \geq 0$ the stabilising solution to the DARE given by

$$\mathbf{X}_s = \mathbf{A}\mathbf{X}_s\mathbf{A}^{\mathrm{T}} - (\mathbf{A}\mathbf{X}_s\mathbf{C}_p^{\mathrm{T}} + \mathbf{S})(\mathbf{C}_p\mathbf{X}_s\mathbf{C}_p^{\mathrm{T}} + \mathbf{R})^{-1}(\mathbf{A}\mathbf{X}_s\mathbf{C}_p^{\mathrm{T}} + \mathbf{S})^{\mathrm{T}} + \mathbf{Q}, \tag{A.5}$$

with

$$\mathbf{Q} = \mathbf{B}_s\mathbf{B}_s^{\mathrm{T}}, \quad \mathbf{R} = \mathbf{D}_{ps}\mathbf{D}_{ps}^{\mathrm{T}}, \quad \mathbf{S} = \mathbf{B}_s\mathbf{D}_{ps}^{\mathrm{T}}. \tag{A.6}$$

It can be shown that a state-space realisation of the pseudo-inverse $\mathbf{G}_{ps,co}^{\dagger}$ of the co-outer factor is given by [24]

$$\mathbf{G}_{ps,co}^{\dagger} \sim \left[\begin{array}{c|c} \mathbf{A}-\mathbf{K}\mathbf{C}_p & \mathbf{K} \\ \hline -\mathbf{D}_{ps}^{co\dagger}\mathbf{C}_p & \mathbf{D}_{ps}^{co\dagger} \end{array}\right]. \tag{A.7}$$

Furthermore, let the matrix $\mathbf{Y}_s$ be a lower triangular matrix calculated from a Cholesky factorisation of $\mathbf{X}_s$ in Equation (A.5), such that

$$\mathbf{Y}_s\mathbf{Y}_s^{\mathrm{T}} = \mathbf{X}_s. \tag{A.8}$$

Then the following matrix relationships associated with the outer-inner factorisation of $\mathbf{G}_{ps}$ can be defined [19]

$$\mathbf{B}_s\mathbf{D}_{ps}^{ci\mathrm{T}} + \mathbf{A}\mathbf{Y}_s\mathbf{C}_{ps}^{ci\mathrm{T}} = \mathbf{B}_{ps}^{co} \tag{A.9}$$
$$\mathbf{B}_s\mathbf{B}_{ps}^{ci\mathrm{T}} + \mathbf{A}\mathbf{Y}_s\mathbf{A}_{ps}^{ci\mathrm{T}} = \mathbf{Y}_s \tag{A.10}$$
$$\mathbf{D}_{ps}^{co}\mathbf{C}_{ps}^{ci} = \mathbf{C}_p\mathbf{Y}_s. \tag{A.11}$$

Derivation of causal part of $\mathbf{G}_{vs}\mathbf{G}_{ps,ci}^{*}$

Let state-space realisations of $\mathbf{G}_{vs}$ and $\mathbf{G}_{ps,ci}$ be given by Equations (A.1) and (A.2), respectively, where both realisations are strictly stable, such that the eigenvalues of the matrices $\mathbf{A}$ and $\mathbf{A}_{ps}^{ci} = \mathbf{A} - \mathbf{K}\mathbf{C}_p$ are inside the unit circle. Then a state-space realisation of the causal part of $\mathbf{G}_{vs}\mathbf{G}_{ps,ci}^{*}$ is given by [19]

$$\left[\mathbf{G}_{vs}\mathbf{G}_{ps,ci}^{*}\right]_{+} \sim \left[\begin{array}{c|c} \mathbf{A} & \mathbf{B}_s\mathbf{D}_{ps}^{ci\mathrm{T}} + \mathbf{A}\tilde{\mathbf{Y}}_s\mathbf{C}_{ps}^{ci\mathrm{T}} \\ \hline \mathbf{C}_v & \mathbf{D}_{vs}\mathbf{D}_{ps}^{ci\mathrm{T}} + \mathbf{C}_v\tilde{\mathbf{Y}}_s\mathbf{C}_{ps}^{ci\mathrm{T}} \end{array}\right], \tag{A.12}$$

with $\tilde{\mathbf{Y}}_s$ the solution to the Lyapunov equation

$$\mathbf{A}\tilde{\mathbf{Y}}_s\mathbf{A}_{ps}^{ci\mathrm{T}} + \mathbf{B}_s\mathbf{B}_{ps}^{ci\mathrm{T}} = \tilde{\mathbf{Y}}_s. \tag{A.13}$$

From Equation (A.10), it can be seen that $\tilde{\mathbf{Y}}_s = \mathbf{Y}_s$. Using Equation (A.9), the state space realisation in Equation (A.12) can therefore also be written as

$$\left[\mathbf{G}_{vs}\mathbf{G}^*_{ps,ci}\right]_+ \sim \left[\begin{array}{c|c} \mathbf{A} & \mathbf{B}^{co}_{ps} \\ \hline \mathbf{C}_v & \mathbf{D}^{co}_{vs} \end{array}\right], \tag{A.14}$$

where $\mathbf{D}^{co}_{vs} = \mathbf{D}_{vs}\mathbf{D}^{ci\mathrm{T}}_{ps} + \mathbf{C}_v\mathbf{Y}_s\mathbf{C}^{ci\mathrm{T}}_{ps}$.

Minimal realisation of $\mathbf{H}_o$

From Equations (A.7) and (A.14), a minimal realisation of $\mathbf{H}_o$ in Equation (38) is now given by

$$\mathbf{H}_o \sim \left[\begin{array}{c|c} \mathbf{A} - \mathbf{K}\mathbf{C}_p & \mathbf{K} \\ \hline \mathbf{C}_v - \mathbf{D}^{co}_{vs}\mathbf{D}^{co\dagger}_{ps}\mathbf{C}_p & \mathbf{D}^{co}_{vs}\mathbf{D}^{co\dagger}_{ps} \end{array}\right], \tag{A.15}$$

where

$$\begin{aligned} \mathbf{D}^{co}_{vs}\mathbf{D}^{co\dagger}_{ps} &= \mathbf{D}_{vs}\mathbf{D}^{ci\mathrm{T}}_{ps}\mathbf{D}^{co\dagger}_{ps} + \mathbf{C}_v\mathbf{Y}_s\mathbf{C}^{ci\mathrm{T}}_{ps}\mathbf{D}^{co\dagger}_{ps} \\ &= (\mathbf{D}_{vs}\mathbf{D}^{ci\mathrm{T}}_{ps}\mathbf{D}^{co\mathrm{T}}_{ps} + \mathbf{C}_v\mathbf{Y}_s\mathbf{C}^{ci\mathrm{T}}_{ps}\mathbf{D}^{co\mathrm{T}}_{ps})(\mathbf{D}^{co}_{ps}\mathbf{D}^{co\mathrm{T}}_{ps})^{-1}. \end{aligned} \tag{A.16}$$

Using Equations (A.3), (A.8) and (A.11), and the fact that $\mathbf{D}_{ps} = \mathbf{D}^{co}_{ps}\mathbf{D}^{ci}_{ps}$ as can be seen from Equation (A.2), Equation (A.16) can also be written as

$$\mathbf{D}^{co}_{vs}\mathbf{D}^{co\dagger}_{ps} = (\mathbf{D}_{vs}\mathbf{D}^{\mathrm{T}}_{ps} + \mathbf{C}_v\mathbf{X}_s\mathbf{C}^{\mathrm{T}}_p)(\mathbf{C}_p\mathbf{X}_s\mathbf{C}^{\mathrm{T}}_p + \mathbf{R})^{-1}. \tag{A.17}$$

The state-space realisation in Equation (A.15) can thus also be written as

$$\mathbf{H}_o \sim \left[\begin{array}{c|c} \mathbf{A} - \mathbf{K}\mathbf{C}_p & \mathbf{K} \\ \hline \mathbf{C}_v - \mathbf{M}\mathbf{C}_p & \mathbf{M} \end{array}\right], \tag{A.18}$$

where the matrix $\mathbf{M}$ is given by

$$\mathbf{M} = (\mathbf{D}_{vs}\mathbf{D}_{ps}^{\mathrm{T}} + \mathbf{C}_v\mathbf{X}_s\mathbf{C}_p^{\mathrm{T}})(\mathbf{C}_p\mathbf{X}_s\mathbf{C}_p^{\mathrm{T}} + \mathbf{R})^{-1}. \tag{A.19}$$

List of Figures

A.1 Block diagram of the active noise control problem. 43

A.2 Block diagram of the optimisation problem, with M_p physical sensors and M_v virtual sensors. 44

A.3 Schematic diagram of a the acoustic duct arrangement. 45

A.4 Bode diagram of the estimated 32^{nd} order state-space model of the deterministic part of the plant —, compared to the measured frequency response functions — between the control input signal and the secondary physical (left) and virtual (right) disturbances calculated from the validation data-set. 46

A.5 Real-time estimation performance of virtual sensing algorithm for $u(n) = 0$. — virtual primary disturbance $d_v(n)$ — estimated primary disturbance $\hat{d}_v(n|n)$ — virtual output error $\tilde{\varepsilon}_v(n)$. 47

A.6 Real-time control performance at virtual location after convergence of adaptive algorithm. — primary disturbance $d_v(n)$ — residual virtual error signal while minimising $\hat{e}_v(n|n)$ — residual virtual error signal while minimising $e_v(n)$. 48

A.7 (a) Control performance at physical sensor while minimising $e_p(n)$. — physical primary disturbance $d_p(n)$ — residual physical error signal $e_p(n)$. (b) Control performance at virtual location while while minimising $e_p(n)$. — virtual primary disturbance $d_v(n)$ — residual virtual error signal while minimising $\hat{e}_v(n|n)$ — residual virtual error signal while minimising $e_p(n)$. 49

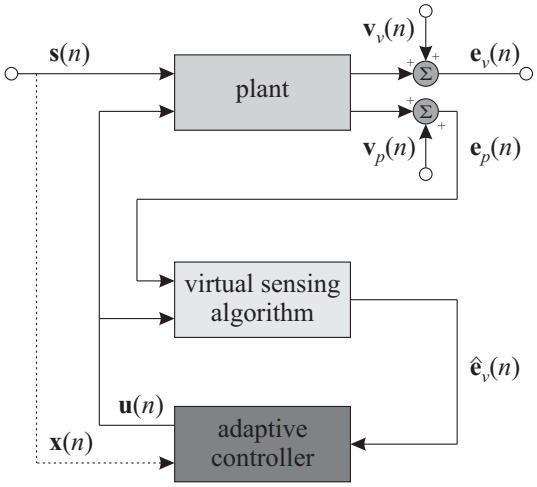

Fig. A.1. Block diagram of the active noise control problem.

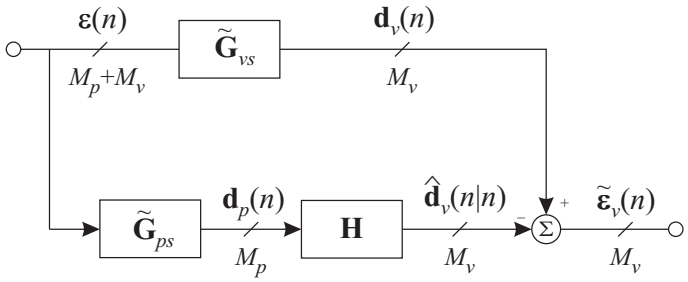

Fig. A.2. Block diagram of the optimisation problem, with M_p physical sensors and M_v virtual sensors.

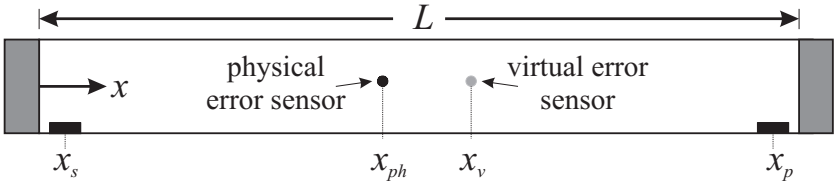

Fig. A.3. Schematic diagram of a the acoustic duct arrangement.

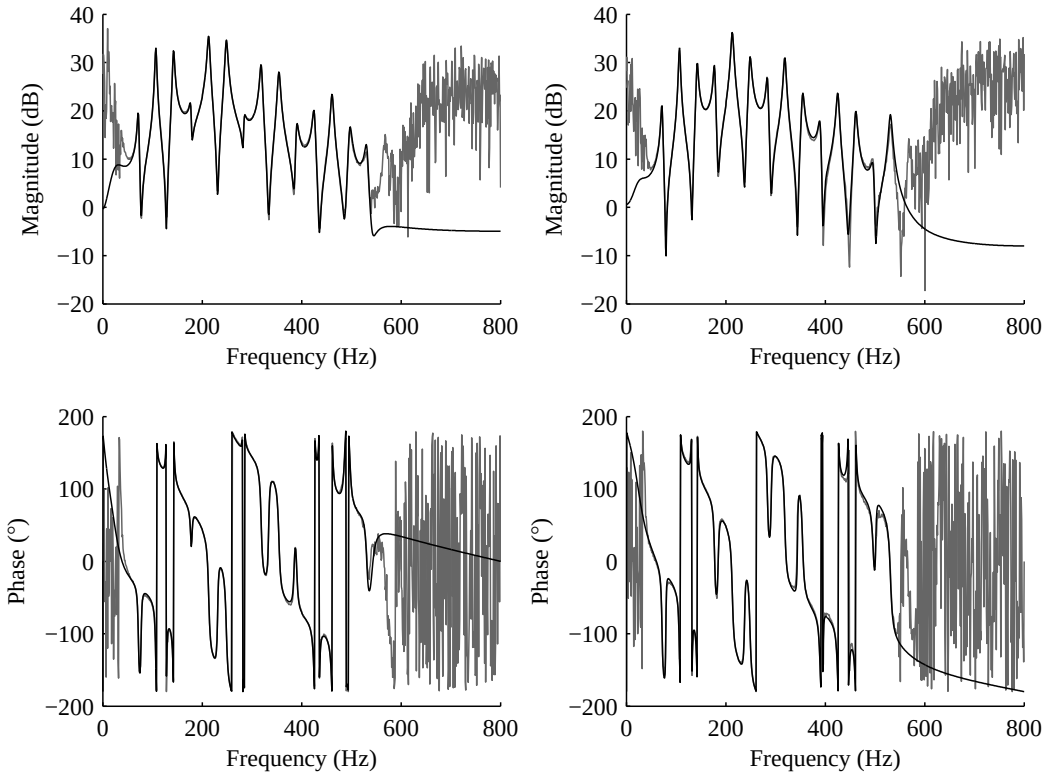

Fig. A.4. Bode diagram of the estimated 32^{nd} order state-space model of the deterministic part of the plant —, compared to the measured frequency response functions — between the control input signal and the secondary physical (left) and virtual (right) disturbances calculated from the validation data-set.

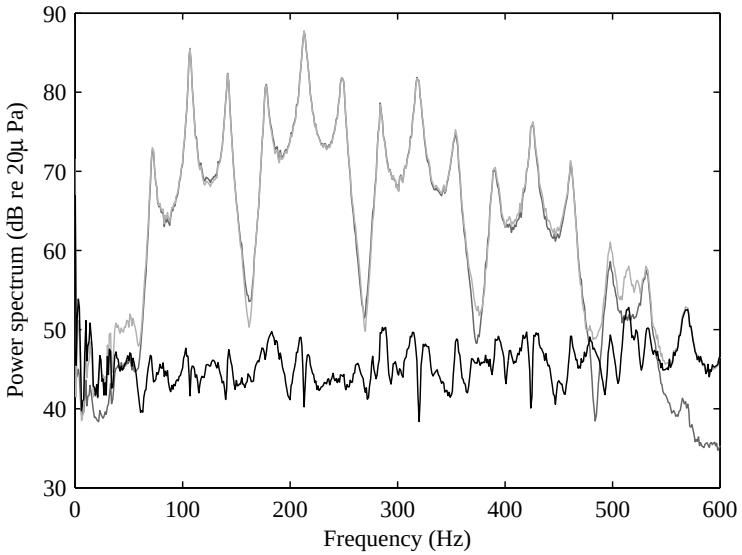

Fig. A.5. Real-time estimation performance of virtual sensing algorithm for $u(n) = 0$. — virtual primary disturbance $d_v(n)$ — estimated primary disturbance $\hat{d}_v(n|n)$ — virtual output error $\tilde{\varepsilon}_v(n)$.

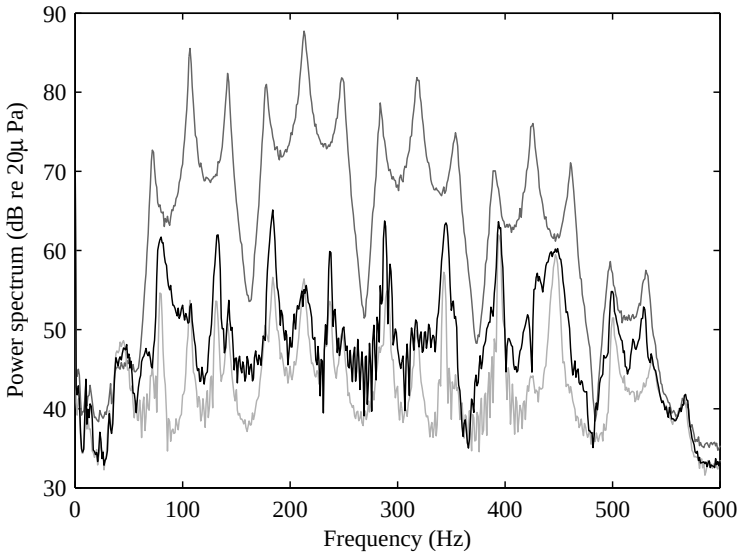

Fig. A.6. Real-time control performance at virtual location after convergence of adaptive algorithm. — primary disturbance $d_v(n)$ — residual virtual error signal while minimising $\hat{e}_v(n|n)$ — residual virtual error signal while minimising $e_v(n)$.

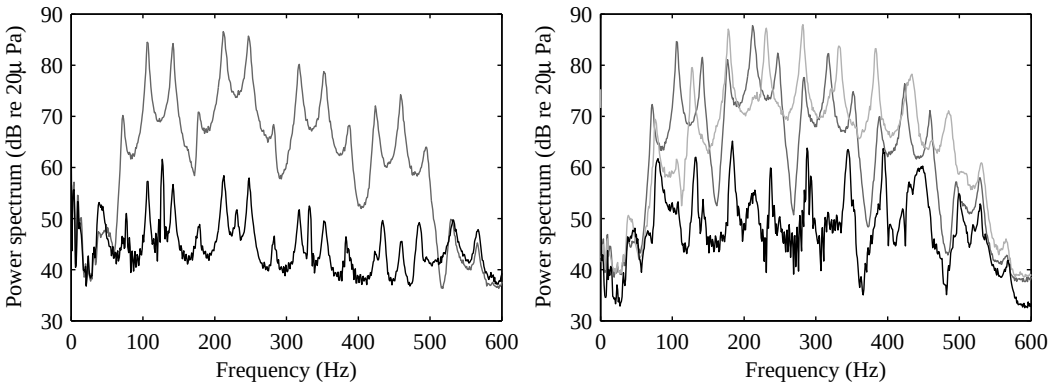

(a) physical sensor (b) virtual sensor

Fig. A.7. (a) Control performance at physical sensor while minimising $e_p(n)$. — physical primary disturbance $d_p(n)$ **—** residual physical error signal $e_p(n)$. (b) Control performance at virtual location while while minimising $e_p(n)$. — virtual primary disturbance $d_v(n)$ **—** residual virtual error signal while minimising $\hat{e}_v(n|n)$ — residual virtual error signal while minimising $e_p(n)$.